

pubs.acs.org/cm Article

Synthesis and Stabilization of Cubic Gauche Polynitrogen under Radio-Frequency Plasma

Haizheng Zhuang, Safa Alzaim, Skywalker Li, El Mostafa Benchafia, Joshua Young, Nuggehalli M. Ravindra, Zafar Iqbal, and Xianqin Wang*



Cite This: Chem. Mater. 2022, 34, 4712–4720



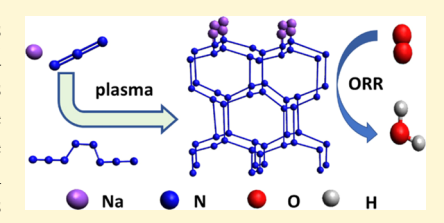
ACCESS I

Metrics & More

Article Recommendations

Supporting Information

ABSTRACT: Cubic gauche polynitrogen (cgPN) has been very attractive because of its high energy density that is 3.5 times of the TNT energy. cgPN has been investigated theoretically in detail, but few experimental studies have been reported. In 2004, cgPN was first synthesized from nitrogen gas under extremely high temperature and high pressure conditions and the trace amount of cgPN in the high-pressure vessel decomposed once the pressure was released. Until recently, our group for the first time synthesized cgPN from an NaN₃ precursor under ambient conditions with radio-frequency plasma. Here, synthesis and stabilization of cgPN are systematically investigated both computationally and



experimentally. The effects of several major factors are studied, and the possible key intermediate is explored. In addition to NaN₃, a ZEZ N₈ precursor is also used. ZEZ N₈ was synthesized by the cyclic voltammetry method. EZE N₈ is found to be the potential intermediate for cgPN formation based on the Fourier transform infrared and Raman spectra and the fact that a higher yield of cgPN is obtained with the ZEZ N₈ precursor. Na⁺ is shown to stabilize cgPN under ambient conditions; however, an excess of Na⁺ has a negative effect on cgPN growth. The oxygen reduction reaction (ORR) was carried out using cgPN as the cathodic catalyst, and the result shows that it is very active for the ORR, which is comparable with a commercial Pt/carbon catalyst. Moreover, cgPN shows an excellent stability during the ORR. This work guides the rational synthesis and scaleup of cgPN and its practical applications for the ORR.

1. INTRODUCTION

During the last few decades, a new group of materials, containing a large number of nitrogen atoms, has been studied. These so-called "high-nitrogen" compounds form a unique class of energetic materials, polynitrogen (PN). In 1985, only molecular nitrogen N₂ and azide anion N₃⁻ were known. Later on, some specific structures of PN were predicted theoretically, such as A7, BP, cg, and nitrogen. Among the structures mentioned above, cubic gauche polynitrogen (cgPN), with cubic symmetry and an I2₁3 space group and comprising a nitrogen network of all single-bonds, is a promising, novel high-energy density material in which the high energy density is due to the significant difference in the average bond between nitrogen-nitrogen single bonds (160 kJ mol⁻¹) and triple bonds (954 kJ mol⁻¹). In 2004, Eremets et al. famously produced a crystalline cg phase: the experimental setup was a diamond anvil cell, with molecular nitrogen as the precursor, a pressure of about 110 GPa, and a temperature of 2000 K. Above 150 GPa, the cgPN phase transitions to a layered PN structure.3 cgPN consists of fused rings of N atoms connected with single bonds, forming a threefold-coordinated polymeric phase⁴ in which the bond length is predicted to be 1.40 Å and the bond angle is 114.0°. The cgPN unit cell contains eight N atoms, with a 3.773 Å lattice constant. It belongs to the I2₁3 space group, having a body-centered-cubic Bravais lattice and a four-atom primitive cell where all bonds are covalent. It is worth pointing out that the bond length and lattice constant decrease with increasing pressure.7 Meanwhile, the vibration frequencies generally increase with increasing pressure, which corresponds to the strengthening of nitrogen single bonds.7 cgPN is transparent in visible light and is characterized by a wide band gap;8 the Pippard relations show that the heat capacity, $C_{\rm p}$, varies linearly with thermal expansion and isothermal compressibility.9 At high temperatures, cgPN has a negative thermal expansion coefficient. 10 The strong covalent bonding can be explained by the threefold atomic coordination stabilized by near-tetrahedral sp³-hybridized electronic states.¹¹ The strong bonding accounts for the high stiffness and bulk modulus of over 300 GPa.² At pressure below 50 GPa, the cg phase is extremely stable and is a preferred nitrogen phase.¹² Yu et al. 13 analyzed cgPN for rocket fuel applications and found that while it has an excellent effective impulse, the surface relaxation results in instability under ambient conditions, with a dissociation barrier of 17 kJ mol⁻¹.

Received: March 5, 2022 Revised: April 18, 2022 Published: May 3, 2022





From a previous study, high temperature and high pressure (HTHP) were necessary for the synthesis of PN, and the PN formed at high pressure dissociated when the pressure decreased.2,14 It has been shown that the Raman frequency of the 600 cm⁻¹ optical mode of cg increases under pressure, which in turn can explain the high-pressure thermodynamic properties of the material. 15 As the pressure decreases, the intermolecular interactions increase in magnitude, becoming comparable to the intramolecular interactions, which results in dissociation of the structure and the decrease of the bulk modulus at low pressure. 16 Zhang et al. 17 studied the (100), (111), and (110) indices of the cg structure, through firstprinciple calculations, finding them to be metastable under ambient conditions; furthermore, this stability could be improved by hydrogen passivation. On the other hand, Eremets et al.² and Caracas⁶ found that at high pressure the (110) reflection index is far more intense than the observed (200) reflection, which is in turn much more intense than the (211) reflection.

In large part, the precursor determines the synthesis conditions. The HTHP requirements in the original experiment of Erba et al. can be attributed to the high barrier to dissociate the triple-bonded N₂. ¹⁸ In contrast to the N₂ precursor of Eremets, Popov¹⁹ used sodium azide as a precursor, in a similar diamond anvil cell setup, because sodium azide has a lower active energy barrier than nitrogen gas²⁰ and a high nitrogen content. The experimental conditions consisted of room temperature and 50 GPa of pressure. The IR and Raman spectra indicated the product to be cgPN. Eremets and co-workers²⁰ also investigated the use of sodium azide as a precursor, finding that, with high pressure above 120 GPa, sodium azide dissociates to form an amorphous nitrogen phase which with laser heating forms clusters that transition to crystalline states. In situ work by Zhu et al.²¹ showed that, below 52 GPa, NaN₃ in a diamond anvil cell undergoes phase transitions, which changes the symmetric azide structure but does not cause its dissociation.

A recent development in the synthesis of cgPN is the use of nonthermal plasma.^{22,23} Plasma is a partially ionized and electrically neutral gas, consisting of electrons, ions, molecules, radicals, photons, and other excited species.²⁴ Because of these high-energy particles, plasma is a powerful tool for material preparation. Compared to conventional thermal approaches, plasma techniques have several advantages, such as high reactivity, rapid reaction, a weak heating effect, a unique effect of electric field introduced on material surfaces, and low possibility to be contaminated by impurities. ²⁵ The conditions of nonthermal plasma are nearly ambient, a vast improvement over the HTHP conditions of the diamond anvil cell. Benchafia et al.²³ employed this technique with an NaN₃ precursor, in contrast to the nitrogen gas precursor of the diamond anvil cell. The (110), (211), and (220) indices were found to have comparable intensities under X-ray diffraction (XRD), in contrast to their differing magnitudes in high-pressure synthesis. While Eremets et al. 26 found the cgPN to grow in single crystals, the plasma technique may present a different growth sequence.

Another new method for PN synthesis is cyclic voltammetry (CV).²⁷ CV is a facile method and can be carried out under ambient conditions. N_8^- prepared using CV has been shown to be an excellent catalyst for the oxygen reduction reaction (ORR).^{27–29} Carbon nanotubes (CNTs) have been found to stabilize PN^{30} and are thus good substrates for N_8^- . In this

study, the mechanism for cgPN synthesis through NaN_3 is investigated. The N_8^- synthesized by CV is also used as a precursor for cgPN synthesis with radio-frequency (RF) plasma.

2. EXPERIMENTAL SECTION

2.1. Preparation of cgPN. Multiwalled carbon nanotube (MWCNT) (purchased from Cheap Tubes Inc.) sheets were prepared following our previous work. Briefly, the MWCNTs were mixed with sodium dodecyl sulfate surfactant. Then the mixture was dispersed into deionized water and sonicated for 30 min followed by a vacuum filtration process to produce CNT sheets. Two pieces of CNT sheets were connected to the positive and negative electrodes, respectively. The MWCNT sheets were dipped in 50 mL NaN₃-H₂O solution which was used as the electrolyte and nitrogen source. Ag/AgCl was used as the standard reference electrode. A constant voltage of 0.5 V was added between positive and negative electrodes for 4 h to separate sodium and azide ions partially. The CNT sheets were taken out, dried in air overnight, and denoted as NaN₃-CNT-pos and NaN₃-CNT-neg. The CNT sheet dipped in the NaN₃ solution was denoted as the NaN₃-CNT-dipped sheet.

 $\rm N_8^-$ electrolytic synthesis was performed on CNT sheets by CV with a computer-controlled three-electrode setup (CH Instruments, 832C Electrochemical Analyzer) in accordance with the previous work. 27 The CNT sheet was connected to the working electrode and dipped in 60 mL NaN3-buffer solution (pH 4.0) with a concentration of 2 M. Pt and Ag/AgCl were used as the counter electrode and standard reference electrode, respectively. The sample was denoted as $\rm N_9\text{-}CNT$.

cgPN synthesis was performed by plasma treatment with a plasma system of 500 watts from Across International (Livingston, NJ, USA). NaN $_3$ powder, NaN $_3$ -CNT-dipped, or N $_8$ -CNT sheets were put into the quartz tube. A mechanical vacuum pump was used to evacuate the reactor. Argon was maintained at a flow rate of 20 standard cubic centimeters per minute (sccm) and a power of 100 W. The reaction time was set to 2 h.

PN is potentially energetic but very stable up to 400 $^{\circ}$ C with or without a substrate; 23,27 protocols will therefore be set up for its safe synthesis. Briefly, the synthesis was carried out in a fume hood. The precursor loaded in the plasma system was highly dispersed on a glass plate and the amount was in the milligram range. Meanwhile, the flowing inert gas (N_2 or Ar) carries heat away during the synthesis.

- **2.2. Preparation of the cgPN Electrode.** Ten milligrams of CNT powder was ultrasonically dispersed in 5 mL ethanol containing a Nafion solution (0.5 wt %, DuPont). Then, 5 μ L of the prepared ink was coated onto the surface of a prepolished glassy carbon electrode (GCE, 3.0 mm) denoted as CNT-GCE and dried in air. Then, the GCE was dipped in 40 mL of 2 M NaN₃ (Aldrich)-H₂O solution or cgPN-H₂O solution overnight. Herein, the samples were denoted as NaN₃-CNT-GCE and cgPN-CNT-GCE, respectively. The resulting NaN₃-CNT-GCE and cgPN-CNT-GCEs were dried in air and used as the working electrodes for ORR tests.
- **2.3. Characterization.** Fourier transform infrared (FTIR) spectroscopy measurements were performed using a Magna Model 560 instrument (Nicolet Instrument Corporation, Madison, WI, USA) attached to an attenuated total reflectance (ATR) accessory with a reflection diamond crystal (Pike Technologies, Madison, WI, USA). Measurements of Raman spectra were carried out with a Thermo Scientific DXR micro-Raman spectrometer (Thermo Scientific, Waltham, MA, USA) with 532 nm laser excitation at a spectral resolution of 2 cm⁻¹ and a spatial resolution of 10 μ m. XRD measurements were conducted with a Philips PW3040 X-ray Diffractometer in the range from 10 to 90° with $\text{CuK}\alpha$ radiation ($\mathring{\lambda}$ = 1.54 Å) with a step size of 0.02°. Temperature-programmed desorption (TPD) tests were carried out using an AutoChem II 2920 system. Samples were heated in flowing helium from room temperature to 800 °C at a heating rate of 10 °C min⁻¹. The released species were monitored with an online mass spectrometer (QMS 200, Stanford Research Systems). Ammonia was determined

by UV—vis spectrophotometry at 420 nm using a Cary 300 UV—vis spectrophotometer (Agilent Technologies, Budd Lake, NJ, USA) using sodium potassium tartrate and Nessler's reagent in accordance with the previous literature.³¹

2.4. Electrochemical Measurement. The rotating disk electrode setup (ALS Co., Ltd., Tokyo, Japan) was employed to perform ORR tests while linear sweep voltammetry (LSV) measurements were carried out. For LSV measurements, the scanning rate was 5 mV s⁻¹ with various rotating speeds. The cgPN-CNT-GCE (or NaN₃-CNT-GCE) was used as the working electrode. Pt and Ag/AgCl were used as the counter electrode and reference electrode, respectively. KOH solution (0.1 M) was used as the electrolyte. Prior to the tests, oxygen or nitrogen was bubbled into the electrolyte for at least 30 min until saturation; during the experiments, oxygen or nitrogen was continuously flowed into the electrolyte to maintain saturation. The control experiment over 10 wt % Pt/C was also performed. The potentials were converted to reversible hydrogen electrode (RHE) scale with the following equation: $E(RHE) = E(Ag/AgCl) + 0.991 V.^{32}$

2.5. Computational Methods. Spin polarized density functional theory (DFT) calculations were carried out using the Vienna ab initio simulation package³³ using the projector augmented wave method³⁴ and the Perdew-Burke-Ernzerhof formulation of the generalized gradient approximation as the functional.³⁵ First, the lattice parameters and atomic positions of the bulk cgPN crystal structure (space group I2₁3) were optimized using an $18 \times 18 \times 18 \Gamma$ -centered k-point mesh and 1000 eV plane wave cutoff until the changes in the forces were less than 0.005 eV Å⁻¹. The energy was considered to be self-consistent when the energy change was smaller than 10⁻⁶ eV. Dispersion interactions were included using Grimme's DFT-D3 methodology.³⁶ One-hundred and thirty two and 152 atom supercells of cgPN (110) and (211) surfaces were considered in these simulations. This ensured that, upon adsorption of Na, the periodic images would be separated by more than 10 Å. A vacuum region of 20 Å was inserted above the surface termination in the out-of-plane direction. Selective dynamics was used to freeze the bottom layer to simulate the bulk, while the rest of the layers were allowed to fully relax. The surfaces were optimized using a $2 \times 2 \times 1$ Γ -centered kpoint mesh and 1000 eV plane wave cutoff until the changes in the forces were less than 0.01 eV Å⁻¹. The energy was considered to be self-consistent when the energy change was smaller than 10^{-6} eV. Bader charge calculations were performed using the method of Henkelman et al.³⁷ The surface energy was calculated using the equation:

$$E_{\text{surf}} = (E_{\text{supercell}} - nE_{\text{bulk}} - xE_{\text{Na}})/2A \tag{1}$$

where $E_{
m supercell}$ is the energy of the relaxed surface, $E_{
m bulk}$ is the energy of cgPN, n is the number of cgPN formula units in the supercell, $E_{
m Na}$ is the energy of an Na atom, x is the number of Na in the system, and A is the surface area.

3. RESULTS AND DISCUSSION

3.1. Plasma Treatment with Varying Time. The evolution in the cgPN synthesis is indicated by the ATR-FTIR spectra for the NaN₃-CNT after plasma treatment over time. ATR-FTIR spectra of samples after interaction with plasma are depicted in Figure 1. Before the plasma treatment, only the peak at 2100 cm⁻¹ of the NaN₃ spectrum can be observed. New peaks, after reaction with plasma, are at 1428 and 880 cm⁻¹. The peak at 880 cm⁻¹ is assigned to cgPN at ambient pressure, while the peak at 1428 cm⁻¹ is assigned to the azide ions in phase I.²³ The structure of phase I, from the work of Eremets et al., is a nitrogen network with intercalated azide ions.²⁰ In addition to these major peaks, there are several minor peaks, such as the peaks at 965, 1201, 1531, and 2210 cm⁻¹ in the samples after interaction with plasma. The minor peaks match the calculation results of EZE N₈.³⁸ Thus, N₈ is

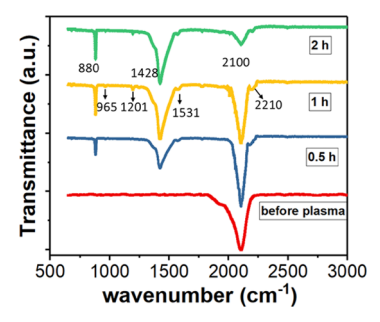


Figure 1. ATR-FTIR spectra of the samples NaN_3 -CNT-dipped before and after varying time of plasma treatment.

the potential intermediate product of the reaction from N_3^- to cgPN.

The Raman spectra of samples produced by the plasma reaction as a function of time are shown in Figure 2. Three

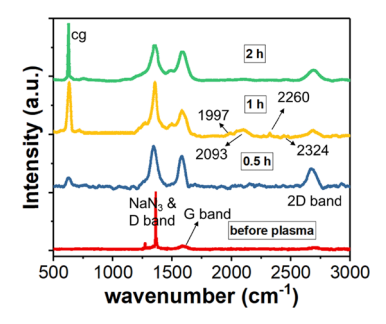


Figure 2. Raman spectra of the samples NaN₃-CNT-dipping before and after different times of reaction with plasma.

typical peaks of CNTs, D-band at 1340 cm⁻¹, G-band at 1570 cm⁻¹, and 2D band at 2620 cm⁻¹, are observed in all samples.³⁹ In addition, the peaks at 1267 and 1360 cm⁻¹ are assigned to the $2\nu_2$ and ν_1 modes of the azide ion, respectively.²³ After the plasma reaction of NaN₃-CNT-dipping, the following new peaks are observed: a strong peak at 637 cm⁻¹, two broad peaks at 1997 and 2093 cm⁻¹, and two weak peaks at 2260 and 2324 cm⁻¹.

The peak at $637~\rm cm^{-1}$ is assigned to cgPN.²³ The new Raman peaks at $1997~\rm cm^{-1}$ can be assigned to vibrations of the nitrogen network in phase I and $2093~\rm cm^{-1}$ can be assigned to the Raman activated ν_3 vibration of the azide ions intercalated in the phase I structure.²³ The peak at $2325~\rm cm^{-1}$, in the plasma-reacted samples, is attributed to nitrogen trapped in the CNTs.²³ The new Raman peak at $2260~\rm cm^{-1}$ can be assigned to EZE N_8 ,³⁸ which confirms that EZE N_8 is the intermediate in the reaction with the plasma. It is unlike the transformation from N_2 to cgPN, at high temperature and high pressure, where the nitrogen goes through an amorphous phase.⁴⁰ However, the peak at $2260~\rm cm^{-1}$ is weak but appears in all the samples, which may indicate that EZE N_8 is an important, but unstable intermediate product, which cannot exist in large quantities.

It is worth noting that the reaction time depends on the power of the plasma and the position of the sample in the reactor, while the product is always cgPN. The product is determined by the precursor and experimental conditions. In RF plasma, the ion density exhibits a large peak in the intense zone, and a lower density plasma is present both upstream and downstream (low-intensity zones). Additionally, for the

cross-section distribution, the ion density is highest at the radial center. However, while the electron density varies, the electron energy is similar at different axial or radial positions. The major interaction in the system is between the sample and the electrons. Therefore, even though the reaction times are different, the system always results in cgPN.

Moreover, even though the bulk temperature of the plasma can be at room temperature, the sample in the reactor may be at hundreds of Kelvins because of the collisions between hot electrons and molecules. The collisions dissociate and ionize the precursors, producing highly reactive radicals and ions. These radicals and ions react exothermally on the sample surfaces, which heat the sample to a higher temperature. While high temperature may cause PN decomposition, high electron density leads to a high yield of PN in a certain time. Thus, the sample location with an appropriate density of electrons in the reactor is critical but difficult to determine.

3.2. Particle-Size Effect. The NaN₃ powders with different particle sizes, <150, 150 \sim 250, and >250 μ m, were treated with Ar plasma for 2 h at a power of 100 W. XRD patterns from NaN₃ powder, before and after reaction plasma, are shown in Figure 3. The peaks near the 2θ value of 66 and 77° are

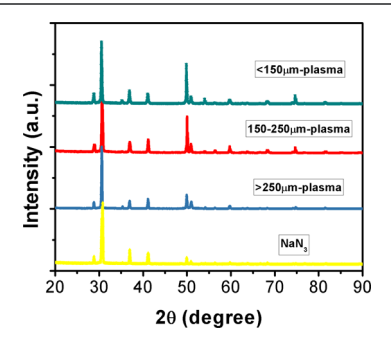


Figure 3. XRD patterns of NaN₃ before plasma treatment and NaN₃ with a particle size of <150, 150 \sim 250, and >250 μ m after plasma treatment.

assigned to the (211) and (220) reflections from the cgPN structure, while the other peaks are from NaN3.2 comparing the peak intensity, the ratios of cg to NaN3 are 6.7:100, 2.9:100, and 1.2:100 corresponding to the particle size of <150, 150 \sim 250, and >250 μ m, respectively. This shows that the sample with a higher specific area, after plasma treatment, achieved a higher yield of cgPN. Therefore, the specific area is important for the reaction with the plasma. On the one hand, diffusion is a limiting step for the chemical reaction and the ions on the surface have a lower migration energy barrier. 44 The sample with a smaller size is heated to a higher temperature because of the small heat capacity, which in turn facilitates the diffusion of radicals on the sample surface. On another hand, the plasma interaction might only happen on the sample surface.²⁵ As a result, the sample with a smaller size shows a better result.

3.3. CNT Sheets Soaking in NaN₃ Solution from 1 to 3 M. To increase the specific area of NaN₃, NaN₃ was dispersed on CNT sheets by soaking CNT sheets in NaN₃ solution with varying concentrations of 1, 2, and 3 M. As shown in Table 1, with increasing azide concentration, the CNT sheets gained more weight of azide. Meanwhile, in the XRD patterns (Figure 4), the relative intensity of NaN₃ at 31° to CNTs at 27° increased, while the relative intensity of cgPN at 77° to NaN₃ at 31° decreased from NaN₃-CNT-plasma-1 M to NaN₃-CNT-

Table 1. Mass Change of CNT Sheets after Soaking in NaN_3 Solution with Different Concentrations and the Volume Ratio of cgPN to NaN_3 after Plasma Treatment According to the XRD Pattern

sample label	CNT sheet mass gain after soaking in NaN_3 solution	volume ratio of cgPN to NaN ₃
NaN ₃ -CNT- plasma-1 M	47.4%	1.60
NaN ₃ -CNT- plasma-2 M	78.7%	0.83
NaN ₃ -CNT- plasma-3 M	120%	0.49

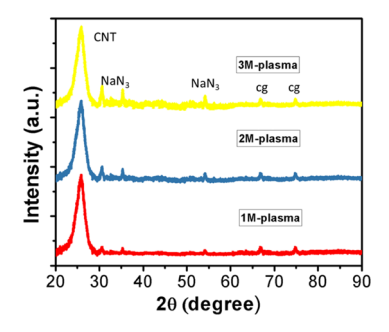


Figure 4. XRD patterns of NaN_3 -CNT-plasma-1 M, NaN_3 -CNT-plasma-2 M, and NaN_3 -CNT-plasma-3 M sheets after plasma treatment.

plasma-3 M. The results show that, with increasing azide concentration, more azides are adsorbed to CNTs, while the conversion ratio from N_3 to N_8 decreases. This indicates that when the CNT sheet is soaked into the NaN_3 solution with a low concentration, NaN_3 forms a thin layer on CNT and cannot cover CNT completely. Thus, a high ratio of cgPN to NaN_3 is achieved, while the ratio of cgPN to CNT is low. When the concentration is high enough, the electrons from plasma cannot penetrate the NaN_3 layer to cause nitrogen polymerization.

To investigate the thermal stability and determine the amount of cgPN produced, TPD tests were performed on these samples. The mass loss during TPD can be attributed to the dissociation of azide or cgPN into N₂ gas. Three N₂ peaks were detected for the NaN₃-CNT sheets corresponding to azide deposited on the outer-, intra-, and inter-layers of the nanotubes in the CNT sheet. The TPD scans of the NaN₃-CNT sheets, after plasma treatment (Figure 5), show that the cgPN species formed on the CNT substrate is thermally stable with a decomposition temperature of 430–460 °C. No carbon

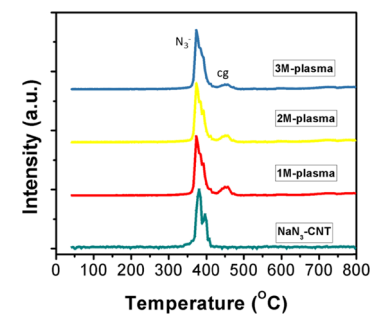


Figure 5. TPD scans of the NaN_3 -CNTs in different concentrations of NaN_3 solution after plasma treatment. The curves were normalized by the sample weight.

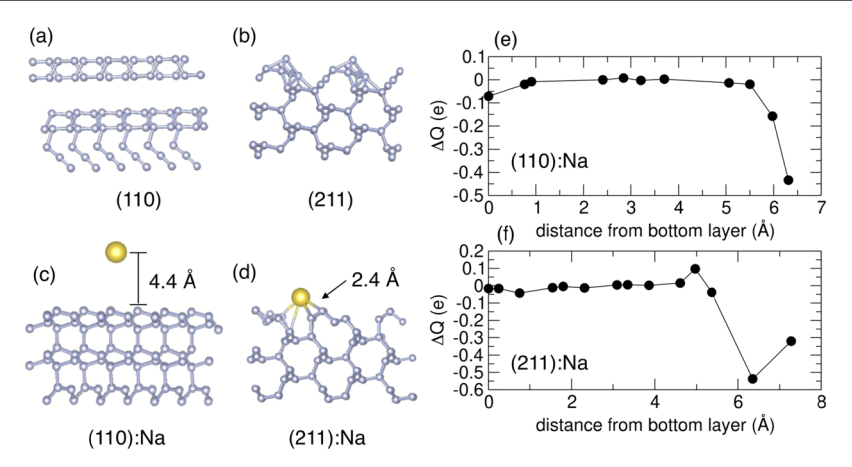


Figure 6. Structure of the DFT-optimized cgPN (a) (110) surface, (b) (211) surface, (c) (110) surface with Na, and (d) (211) surface with Na. Charge transfer (ΔQ) to (e) (110) surface and (f) (211) surface.

nitride species are detected on the cgPN-CNT sheet.²⁷ Moreover, from TPD tests, the percentages of cgPN in the total nitrogen are as follows: 14.1, 9.4, and 6.4% of NaN₃-CNT-1, -2, and -3 M, respectively; these values are much lower than the percentages from XRD results. This is because XRD can just detect the sample under the surface of several micrometers, while TPD can measure the whole sample. It confirms that the reaction with plasma is a surface interaction and cannot cause the structure change for most of NaN₃ beneath the surface of the sample.

3.4. Effect of Na⁺ on cgPN Synthesis. From both experiment and theory, the PN of pure nitrogen synthesized under HTHP tends to decompose to molecular nitrogen because of the instability of PN. ^{2,14,45} The challenge remains to recover and preserve polymeric nitrogen compounds at room temperature and pressure. Nitrogen-rich compounds provide an alternative route to the synthesis of PN with single or double nitrogen bonds under ambient conditions. The heteroatom lowers the polymerization and decomposition pressure. For instance, the heteroatoms, such as Li, 46 Na, 47 Cs,⁴⁸ Ca,⁴⁹ C,⁵⁰ and so on, will enhance the PN stability as an electron donor, which will cause the redistribution of electrons and metallization of the system, resulting in a change in chemical bonding. The competition between ionic and covalent bonding promotes new nitrogen phases other than triply bonded N_2 . From our work, the synthesis of cgPN from NaN3 under ambient conditions shows the stability enhancement of cgPN by Na.

To demonstrate the ability of Na to stabilize cgPN surfaces, DFT calculations were performed. First, (110) and (211) surfaces of cgPN were created and optimized (cf. Methods, Figure 6a,b, respectively). As expected, both surfaces were found to be unstable, with the top layer either breaking apart or completely separating from the bulk. Calculation of the surface energy ($E_{\rm surf}$) results in a value of $-2.01~{\rm J~m^{-2}}$ and $-1.16~{\rm J~m^{-2}}$ for the (110) and (211), respectively. These unphysical negative values of $E_{\rm surf}$ indicate an unstable surface. This is in agreement with Zhang et al., ¹⁷ who demonstrated that the (110) surface is a highly unstable one (we note that they did not investigate the (211) surface).

Next, an Na atom was placed on both surfaces, with several chemisorbed and physisorbed positions checked to determine the most energetically favorable site. On the (110) termination, Na was found to be stable in a physiosorbed configuration at 4.4 Å (Figure 6c), and the (110) surface is

completely stable following optimization; this stabilizing effect is reflected in the now positive $E_{\rm surf}$ values of 0.86 J m⁻² for physisorbed Na on the (110) surface. Interestingly, this position is more stable than any Na chemisorbed position on the surface. On the (211) surface, there was no physisorbed site; following optimization, all such Na positions eventually chemisorbed into a pore on the surface at an average distance of 2.4 Å (Figure 6d). However, as with the (110) case, the presence of Na resulted in no decomposition of the surface upon optimization, and an $E_{\rm surf}$ = 0.65 J m⁻² shows the stability upon Na adsorption.

We then computed the Bader charges to investigate the charge transfer on these surfaces. As expected, the Na has a net charge of +0.87e in both cases (nearly +1), while the (110) and (211) surfaces display a net negative charge. An examination of the layer decomposed change in the Bader charge (i.e., the net change in the charge density in a given layer upon Na adsorption) on the (110) and (211) surface (Figure 6e,f, respectively) yields further insights. First, in both cases, charges on layers far from the surface (and therefore from Na) remain nearly zero. In the (110) case, -0.43e and -0.16e of charge are transferred to the first and second topmost layers. In the (211) case, charge transfer extends similarly into the surface resulting from the chemisorption of Na, although the values (-0.32e)and -0.54e) are larger compared to the physisorption found in the (110) case. These results demonstrate that a stabilizing interaction between Na and the cgPN surfaces likely leads to the observed prevention of the surface decomposition.

Meanwhile, a problem of extra Na needs to be addressed. The sample after Ar plasma treatment became dark blue (Figure S1 in the Supplementary Material), which is consistent with sodium nitride (Na₃N) from the previous study.⁵² Unfortunately, there is not much information for Na₃N in the literature. It is likely that, like the ionic crystal NaCl, the vibration frequency is beyond the range of regular IR and Raman. Nevertheless, it is reasonable to deduce that, similar to lithium nitride (Li₃N), ⁵³ Na₃N reacts with water to produce NaOH and NH₃. On the one hand, pH of NaN₃-H₂O with a concentration of 2 M is 8.6, while pH increases to 9.3 in the NaN₃-plasma water solution. On the other hand, the absorbance of UV-vis spectra at 420 nm is enhanced (Table S1 in Supplementary Material). This enhancement can be assigned to the formation of NH3, because the same UV-vis absorbance requires a much higher concentration of NaN3 than NH₃ (Figure S2 in the Supplementary Material).

Therefore, it is concluded that, in the plasma reaction, most N atoms transition to cgPN, while a small fraction of the nitrogens form Na_3N together with Na. Moreover, the plasma sample does not show the characteristic XRD pattern of Na_3N , which indicates that the Na_3N particles, clusters, or films are too small to be detected by XRD.

If CNTs are charged and soaked in ionic solutions, they should attract ions, adsorb them into their interior, and potentially separate them from the solutions. Therefore, to study the effect of Na⁺ on cgPN synthesis, an external potential was added between positive and negative CNT-paper electrodes in NaN₃ solution. NaN₃-CNT sheets on the positive electrode attracted azides; NaN₃-CNT sheets on the negative electrode attracted Na. The results were compared to NaN₃-CNT-dipped without external voltage. The weight change of the CNT samples after external-0.5 V/dipping in NaN₃ solution and nitrogen content is shown in Table 2. The

Table 2. Mass Change of NaN₃-CNT-pos, NaN₃-CNT-neg, and NaN₃-CNT-Dipping Sheets^a

sample	mass ratio of the gained mass after 0.5 V/dipping	mass ratio of the mass loss during TPD to the gained	nitrogen percentage
label	treatment to CNTs	mass	out of NaN ₃
NaN ₃ - CNT- pos.	80.7%	73.8%	64.6%
NaN ₃ - CNT- neg.	75.8%	56.3%	
NaN ₃ - CNT- dipping	78.7%	63.4%	

^aThe nitrogen desorption amount is calculated by integration of the TPD results and comparison of the peak areas to those from injection of pure nitrogen under the same experimental conditions.

positive electrode gained the most mass because azide is heavier than sodium. The CNT sheet connected to the positive electrode received a higher nitrogen content, which indicates that Na^+ and $\mathrm{N_3}^-$ were separated partially by the external 0.5 V in the solution.

The three samples, with different Na concentrations, were then treated by RF plasma (Figure 7). After plasma treatment, the ratio of cg to the remaining NaN₃ of the NaN₃-CNT-pos, NaN₃-CNT-neg, and NaN₃-CNT-dipping samples was 0.83, 0.67, and 0.75, respectively. These results showed that the material with a higher Na content had a lower cgPN yield. It is consistent with the simulation results under high pressure in which the optimized Na contents are 6 and 12% in Na–N

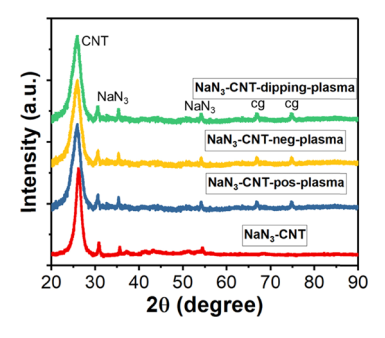


Figure 7. X-ray powder diffraction patterns of NaN₃-CNT-pos, NaN₃-CNT-neg, and NaN₃-CNT-dipping sheets after plasma treatment.

system under 20 and 15 GPa, respectively.⁴⁷ In this case, some Na stabilizes cgPN, while too much Na can break the cg lattice, form clusters which do not facilitate cgPN stabilization, or simply saturate the active sites.

3.5. From N₈ **to cgPN.** cgPN was also synthesized with ZEZ N_8 precursors because it is reasonable to deduce that the energy barrier between EZE N_8 and ZEZ N_8 is much lower than the barrier between N_3 and EZE N_8 . The formation of N_8 on CNT sheets after CV synthesis was confirmed by ATR-FTIR as shown in Figure 8. The peak at 2050 cm⁻¹ was the

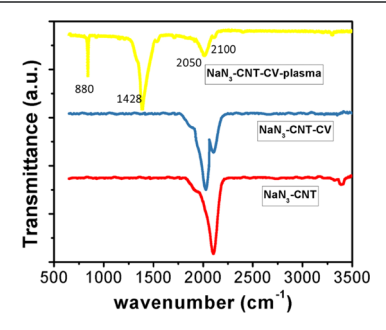


Figure 8. FTIR of the samples after CV and plasma treatment.

characteristic peak of polynitrogen chain ZEZ N_8 , ^{27,28} suggesting that N_8 was synthesized successfully. After plasma treatment, shown by the yellow line, the characteristic IR peak of cgPN at 880 cm⁻¹ is also observed with a strong intensity, indicating the formation of cgPN.

Moreover, as indicated by TPD of Figure 9, N_3 , $N_{8,}$ and cgPN decompose at different temperatures. In addition, by

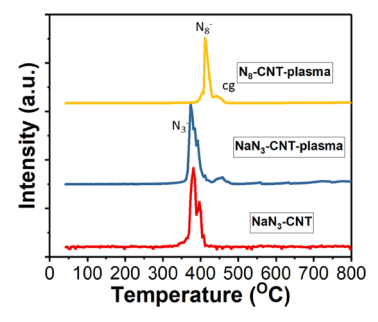


Figure 9. TPD results of NaN $_3\text{-CNT}$, NaN $_3\text{-CNT-plasma}$, and N $_8\text{-CNT-plasma}$.

quantifying the N_2 amount based on the peak area in TPD scans, the cgPN content of 12.6% from N_8 -CNT is higher than the cgPN content of 9.4% from NaN₃-CNT, which shows that N_8 has a higher conversion ratio to cgPN than N_3 . It is consistent with the calculation that N_8 is an important intermediate from N_3 to cgPN, and the transformation from N_3 to N_8 is an essential step.

3.6. Electrocatalytic Performance. The electrocatalytic performance of the cgPN-CNT-GCE in the ORR was investigated by LSV measurements. O₂-saturated 0.1 M KOH was the electrolyte. Prior to each measurement, a background voltammogram was obtained by carrying out the LSV in an N₂-saturated electrolyte, which was subtracted from the value as measured in the O₂-saturated electrolyte. The ORR curves achieved at different rotating speeds are illustrated in Figure 10a. As expected, current density increased with the

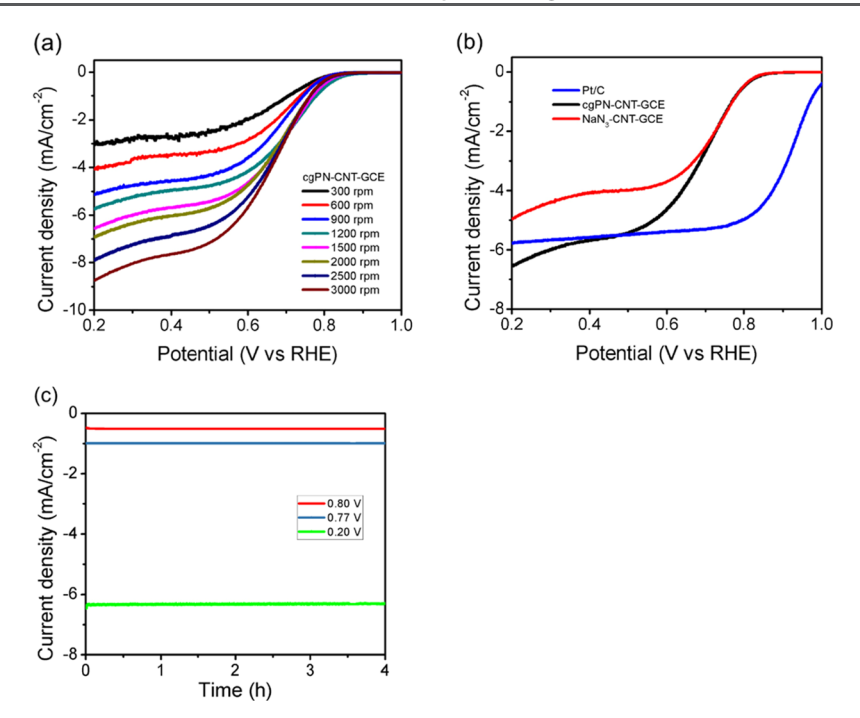


Figure 10. Electrocatalytic performance of cgPN-CNT-GCE, NaN $_3$ -CNT-GCE, and Pt/C-GCE samples. (a) LSV curves of the cgPN-CNT-GCE in an O $_2$ -saturated 0.1 M KOH solution with different rotation speeds at a scan rate of 5 mV s $^{-1}$. (b) LSV curves of the cgPN-CNT-GCE, NaN $_3$ -CNT-GCE, and Pt/C (10 wt % platinum on Vulcan XC-72) in an O $_2$ -saturated 0.1 M KOH solution with a rotation speed of 1500 rpm at a scan rate of 5 mV s $^{-1}$. (c) Long-term test of the cgPN-CNT-GCE at 0.80, 0.77 and 0.20 V, in an O $_2$ -saturated 0.1 M KOH solution with a rotation speed of 1500 rpm.

electrode rotating speed increase, which can be attributed to the enhanced diffusion of electrolytes.

Figure 10b shows the comparison of the current density with a certain rotation speed of 1500 rpm at a scan rate of 5 mV s⁻¹ for all samples. The current density followed the trend of cgPN-CNT-GCE > Pt/C-GCE > NaN3-CNT-GCE at the potential lower than -0.55 V. In consideration of the inferior performance of the NaN3-CNT-GCE, it may be concluded that the enhanced current density originated from the highly active cgPN. Compared to Pt/C, cgPN-CNT has a more negative onset potential of ~0.80 V and half-wave potential of ~0.70 V. However, the cgPN-CNT-GCE has a much higher limiting current density (6.5 mA/cm²) than the Pt/C-GCE (5.8 mA/cm²) commercial catalyst for the ORR. Moreover, the long-term stability of the cgPN-CNT-GCE is evaluated using a chronoamperometric method (Figure 10c). After 4 h of reaction, the current change is negligible, suggesting an excellent stability of cgPN-CNT during the ORR. Without any optimization, cgPN shows superior activity for the ORR and is a potentially good ORR catalyst candidate.

4. CONCLUSIONS

cgPN is synthesized experimentally from NaN_3 and N_8 precursors with and without a CNT substrate with nonthermal RF plasma treatment under ambient conditions. The results show that EZE N_8 is the potential intermediate product from N_3 to cgPN and Na_3N is a byproduct during interaction with plasma. The plasma interacts mainly with the sample surface. Therefore, a higher specific area of the sample also achieves a higher yield of cgPN. In addition, N_8 stabilizes cgPN under ambient conditions, while excess N_8 has a negative effect on the growth of cgPN. ORR experiments suggest that cgPN is active in a basic electrolyte. Although it has a more negative

onset potential and half-wave potential, the current density of the cgPN-CNT-GCE is higher than that of a commercial Pt/C electrode. This work therefore opens the door to the synthesis of cgPN and its potential use as a high-energy and ORR catalytic material.

ASSOCIATED CONTENT

Supporting Information

The Supporting Information is available free of charge at https://pubs.acs.org/doi/10.1021/acs.chemmater.2c00689.

Figure S1: NaN3 after Ar plasma treatment; Figure S2: UV-Vis of NaN3 before and after plasma treatment; Table S1: The absorbance of UV-Vis at 420 nm (PDF)

AUTHOR INFORMATION

Corresponding Author

Xianqin Wang — Department of Chemical and Materials Engineering, New Jersey Institute of Technology, Newark, New Jersey 07102, United States; ⊚ orcid.org/0000-0003-1056-7214; Email: xianqin.wang@njit.edu

Authors

Haizheng Zhuang — Interdisciplinary Program in Materials Science & Engineering, Department of Physics, New Jersey Institute of Technology, Newark, New Jersey 07102, United States

Safa Alzaim — Department of Chemical and Materials Engineering, New Jersey Institute of Technology, Newark, New Jersey 07102, United States

Skywalker Li – Newark Academy, Livingston, New Jersey 07039, United States

El Mostafa Benchafia — Interdisciplinary Program in Materials Science & Engineering, Department of Physics, New

- Jersey Institute of Technology, Newark, New Jersey 07102, United States
- Joshua Young Department of Chemical and Materials Engineering, New Jersey Institute of Technology, Newark, New Jersey 07102, United States
- Nuggehalli M. Ravindra Interdisciplinary Program in Materials Science & Engineering, Department of Physics, New Jersey Institute of Technology, Newark, New Jersey 07102, United States
- Zafar Iqbal Department of Chemical and Materials Engineering, New Jersey Institute of Technology, Newark, New Jersey 07102, United States

Complete contact information is available at: https://pubs.acs.org/10.1021/acs.chemmater.2c00689

Notes

The authors declare no competing financial interest.

ACKNOWLEDGMENTS

This work was supported in part by an NSF CBET-1804949 grant and Department of Physics, New Jersey Institute of Technology.

REFERENCES

- (1) Niu, S.; Liu, S.; Liu, B.; Shi, X.; Liu, S.; Liu, R.; Yao, M.; Cui, T.; Liu, B. High energetic polymeric nitrogen sheet confined in a graphene matrix. *RSC Adv.* **2018**, *8*, 30912–30918.
- (2) Eremets, M. I.; Gavriliuk, A. G.; Trojan, I. A.; Dzivenko, D. A.; Boehler, R. Single-bonded cubic form of nitrogen. *Nat. Mater.* **2004**, *3*, 558–563.
- (3) Cheng, P.; Yang, X.; Zhang, X.; Wang, Y.; Jiang, S.; Goncharov, A. F. Polymorphism of polymeric nitrogen at high pressures. *J. Chem. Phys.* **2020**, *152*, 244502.
- (4) Plašienka, D.; Martoňák, R. Transformation pathways in high-pressure solid nitrogen: From molecular N2 to polymeric cg-N. *J. Chem. Phys.* **2015**, *142*, No. 094505.
- (5) Mailhiot, C.; Yang, L. H.; McMahan, A. K. Polymeric nitrogen. *Phys. Rev. B* **1992**, *46*, 14419–14435.
- (6) Caracas, R. Raman spectra and lattice dynamics of cubic gauche nitrogen. J. Chem. Phys. 2007, 127, 144510.
- (7) Zhao, J. First-principles study of atomic nitrogen solid with cubic gauche structure. *Phys. Lett. A* **2007**, *360*, 645–648.
- (8) Yu, H. L.; Yang, G. W.; Xiao, Y.; Mao, Y. Band structure and optical properties of single-bonded cubic nitrogen: A first-principle study. *Chem. Phys. Lett.* **2006**, 419, 450–453.
- (9) Yurtseven, H.; Tiryaki, Ö.; Tari, O. Pippard relations for cubic gauche nitrogen. *Anadolu Univ. J. Sci. Technol. A Appl. Sci. Eng.* **2016**, *17*, 741–741.
- (10) Yakub, L. Thermodynamics of Solid Polymerized Nitrogen. J. Low Temp. Phys. 2005, 139, 783-789.
- (11) Chen, X.-Q.; Fu, C. L.; Podloucky, R. Bonding and strength of solid nitrogen in the cubic gauche (cg-N) structure. *Phys. Rev. B* **2008**, 77, No. 064103.
- (12) Kotakoski, J.; Albe, K. First-principles calculations on solid nitrogen: A comparative study of high-pressure phases. *Phys. Rev. B* **2008**, *77*, No. 144109.
- (13) Yu, T.; Lai, W.-P.; Liu, Y.-Z.; Wu, B.; Ge, Z.-X.; Bu, J.-H. The outlook for platonic and cubic gauche nitrogens. *Comput. Mater. Sci.* **2016**, *123*, 31–39.
- (14) Laniel, D.; Winkler, B.; Fedotenko, T.; Pakhomova, A.; Chariton, S.; Milman, V.; Prakapenka, V.; Dubrovinsky, L.; Dubrovinskaia, N. High-Pressure Polymeric Nitrogen Allotrope with the Black Phosphorus Structure. *Phys. Rev. Lett.* **2020**, 124, No. 216001.
- (15) Yurtseven, H. H.; Tiryaki, Ö. Pressure dependence of the Raman frequency of an optical mode in cubic gaughe nitrogen.

- International Turkish Congress on Molecular Spectroscopy 2015, 2015, 13-18.
- (16) Akay, Ö.; Yurtseven, H. Investigation of vibrational, elastic and dielectric properties of cubic gauche nitrogen (cg-N). *Optik* **2021**, 236, No. 166481.
- (17) Zhang, T.; Zhang, S.; Chen, Q.; Peng, L. M. Metastability of single-bonded cubic-gauche structure of N under ambient pressure. *Phys. Rev. B* **2006**, *73*, No. 094105.
- (18) Erba, A.; Maschio, L.; Pisani, C.; Casassa, S. Pressure-induced transitions in solid nitrogen: Role of dispersive interactions. *Phys. Rev. B* **2011**, *84*, No. 012101.
- (19) Popov, M. Raman and IR study of high-pressure atomic phase of nitrogen. *Phys. Lett. A* **2005**, 334, 317–325.
- (20) Eremets, M. I.; Popov, M. Y.; Trojan, I. A.; Denisov, V. N.; Boehler, R.; Hemley, R. J. Polymerization of nitrogen in sodium azide. *J. Chem. Phys.* **2004**, *120*, 10618–10623.
- (21) Zhu, H.; Zhang, F.; Ji, C.; Hou, D.; Wu, J.; Hannon, T.; Ma, Y. Pressure-induced series of phase transitions in sodium azide. *J. Appl. Phys.* **2013**, *113*, No. 033511.
- (22) Benchafia, E. M.; Yu, C.; Sosnowski, M.; Ravindra, N. M.; Iqbal, Z. Plasma Synthesis of Nitrogen Clusters on Carbon Nanotube Sheets. *JOM* **2014**, *66*, 608–615.
- (23) Benchafia, E. M.; Yao, Z.; Yuan, G.; Chou, T.; Piao, H.; Wang, X.; Iqbal, Z. Cubic gauche polymeric nitrogen under ambient conditions. *Nat. Commun.* **2017**, *8*, 930.
- (24) Wang, Z.; Zhang, Y.; Neyts, E. C.; Cao, X.; Zhang, X.; Jang, B. W. L.; Liu, C.-J. Catalyst Preparation with Plasmas: How Does It Work? ACS Catal. 2018, 8, 2093–2110.
- (25) Ouyang, B.; Zhang, Y.; Xia, X.; Rawat, R. S.; Fan, H. J. A brief review on plasma for synthesis and processing of electrode materials. *Mater. Today Nano* **2018**, *3*, 28–47.
- (26) Eremets, M. I.; Gavriliuk, A. G.; Trojan, I. A. Single-crystalline polymeric nitrogen. *Appl. Phys. Lett.* **2007**, *90*, 171904.
- (27) Wu, Z.; Benchafia el, M.; Iqbal, Z.; Wang, X. N8 polynitrogen stabilized on multi-wall carbon nanotubes for oxygen-reduction reactions at ambient conditions. *Angew. Chem., Int. Ed.* **2014**, *53*, 12555–12559.
- (28) Yao, Z.; Hu, M.; Iqbal, Z.; Wang, X. N8— Polynitrogen Stabilized on Boron-Doped Graphene as Metal-Free Electrocatalysts for Oxygen Reduction Reaction. ACS Catal. 2020, 10, 160–167.
- (29) Yao, Z.; Fan, R.; Ji, W.; Yan, T.; Hu, M. N8– Polynitrogen Stabilized on Nitrogen-Doped Carbon Nanotubes as an Efficient Electrocatalyst for Oxygen Reduction Reaction. *Catalysts* **2020**, *10*, 864
- (30) Abou-Rachid, H.; Hu, A.; Timoshevskii, V.; Song, Y.; Lussier, L.-S. Nanoscale High Energetic Materials: A Polymeric Nitrogen Chain N8 Confined inside a Carbon Nanotube. *Phys. Rev. Lett.* **2008**, *100*, No. 196401.
- (31) Qin, M.; Li, X.; Gan, G.; Wang, L.; Fan, S.; Yin, Z.; Chen, G. Boosting Electrocatalytic Nitrogen Fixation with Co–N3 Site-Decorated Porous Carbon. ACS Sustainable Chem. Eng. 2020, 8, 13430–13439.
- (32) Wang, L.; Lee, C.-Y.; Schmuki, P. Solar water splitting: preserving the beneficial small feature size in porous α -Fe2O3 photoelectrodes during annealing. *J. Mater. Chem. A* **2013**, *1*, 212–215.
- (33) Kresse, G.; Furthmüller, J. Efficient iterative schemes for ab initio total-energy calculations using a plane-wave basis set. *Phys. Rev.* B **1996**, *54*, 11169–11186.
- (34) Blöchl, P. E. Projector augmented-wave method. *Phys. Rev. B* **1994**, *50*, 17953–17979.
- (35) Perdew, J. P.; Burke, K.; Ernzerhof, M. Generalized Gradient Approximation Made Simple. *Phys. Rev. Lett.* **1996**, 77, 3865–3868.
- (36) Grimme, S.; Antony, J.; Ehrlich, S.; Krieg, H. A consistent and accurate ab initio parametrization of density functional dispersion correction (DFT-D) for the 94 elements H-Pu. *J. Chem. Phys.* **2010**, 132, 154104.

- (37) Henkelman, G.; Arnaldsson, A.; Jónsson, H. A fast and robust algorithm for Bader decomposition of charge density. *Comput. Mater. Sci.* **2006**, *36*, 354–360.
- (38) Bartlett, R.; Fau, S.; Tobita, M.; Wilson, K.; Perera, A. Structure and Stability of Polynitrogen Molecules and Their Spectroscopic Characteristics, Quantum Theory Project, Report (AFOSR-DARPA (F49620-98-1-0477)); University of Florida, 2001. https://www.researchgate.net/publication/2403823_Structure_and_Stability_of_Polynitrogen_Molecules_and_Their_Spectroscopic_Characteristics.
- (39) Zeng, X.; Wang, Z.; Meng, N.; McCarthy, D. T.; Deletic, A.; Pan, J.-H.; Zhang, X. Highly dispersed TiO2 nanocrystals and carbon dots on reduced graphene oxide: Ternary nanocomposites for accelerated photocatalytic water disinfection. *Appl. Catal., B* **2017**, 202, 33–41.
- (40) Trojan, I. A.; Eremets, M. I.; Medvedev, S. A.; Gavriliuk, A. G.; Prakapenka, V. B. Transformation from molecular to polymeric nitrogen at high pressures and temperatures: In situ x-ray diffraction study. *Appl. Phys. Lett.* **2008**, *93*, No. 091907.
- (41) Uner, N. B.; Thimsen, E. Low temperature plasma as a means to transform nanoparticle atomic structure. *Plasma Sources Sci. Technol.* **2018**, 27, No. 074005.
- (42) Blackwell, D. D.; Chen, F. F. Two-dimensional imaging of a helicon discharge. *Plasma Sources Sci. Technol.* **1997**, *6*, 569–576.
- (43) Kortshagen, U. R.; Sankaran, R. M.; Pereira, R. N.; Girshick, S. L.; Wu, J. J.; Aydil, E. S. Nonthermal plasma synthesis of nanocrystals: Fundamental principles, materials, and applications. *Chem. Rev.* **2016**, *116*, 11061–11127.
- (44) Wang, Q.; Ma, Y.; Sang, D.; Wang, X.; Liu, C.; Hu, H.; Wang, W.; Zhang, B.; Fan, Q.; Han, Y.; et al. Ionic conduction in sodium azide under high pressure: Experimental and theoretical approaches. *Appl. Phys. Lett.* **2018**, *112*, 173903.
- (45) Melicherová, D.; Kohulák, O.; Plašienka, D.; Martoňák, R. Structural evolution of amorphous polymeric nitrogen from ab initio molecular dynamics simulations and evolutionary search. *Phys. Rev. Mater.* **2018**, *2*, No. 103601.
- (46) Laniel, D.; Weck, G.; Loubeyre, P. Direct Reaction of Nitrogen and Lithium up to 75 GPa: Synthesis of the Li3N, LiN, LiN2, and LiN5 Compounds. *Inorg. Chem.* **2018**, *57*, 10685–10693.
- (47) Cormier, M. M. E.; Bonev, S. A. Polymerization of sodium-doped liquid nitrogen under pressure. *Phys. Rev. B* **2017**, *96*, No. 184104.
- (48) Wang, X.; Li, J.; Zhu, H.; Chen, L.; Lin, H. Polymerization of nitrogen in cesium azide under modest pressure. *J. Chem. Phys.* **2014**, *141*, No. 044717.
- (49) Zhu, S.; Peng, F.; Liu, H.; Majumdar, A.; Gao, T.; Yao, Y. Stable Calcium Nitrides at Ambient and High Pressures. *Inorg. Chem.* **2016**, *55*, 7550–7555.
- (50) Strout, D. Effect of C-O Bonding on the Stability and Energetics of High-Energy Nitrogen-Carbon Molecules N 10 C 2 and N 16 C 2. Adv. Chem. 2014, 2014, 1-7.
- (51) Steele, B. A.; Oleynik, I. I. Computational Discovery of New High-Nitrogen Energetic Materials. In *Computational Approaches for Chemistry Under Extreme Conditions*, Goldman, N. Ed.; Springer International Publishing, 2019; 25–52.
- (52) Vajenine, G. V. Plasma-Assisted Synthesis and Properties of Na3N. *Inorg. Chem.* **2007**, *46*, 5146–5148.
- (53) Gregory, D. H. Lithium nitrides, imides and amides as lightweight, reversible hydrogen stores. *J. Mater. Chem.* **2008**, *18*, 2321–2330.
- (54) Yzeiri, I.; Patra, N.; Král, P. Porous carbon nanotubes: Molecular absorption, transport, and separation. *J. Chem. Phys.* **2014**, 140, 104704.

☐ Recommended by ACS

Insights into the Mechanism of Elemental Mercury Adsorption on Graphitic Carbon Nitride: A Density Functional Theory Study

Yang Ling, Dongjing Liu, et al.

MAY 21, 2021 ENERGY & FUELS

READ 🗹

Unraveling the Structure of the Poly(triazine imide)/LiCl Photocatalyst: Cooperation of Facile Syntheses and a Low-Temperature Synchrotron App...

Chang-Zhong Liao, Kaimin Shih, et al.

NOVEMBER 13, 2019

INORGANIC CHEMISTRY

READ 🗹

Graphitic Carbon Nitride Codoped with Sulfur and Yttrium for Efficient Visible-Light Photocatalytic Performance

Xin Bai, Yongping Zhang, et al.

NOVEMBER 19, 2021

ACS APPLIED ENERGY MATERIALS

READ 🗹

Spatial Separation of Charge Carriers via Heterogeneous Structural Defects in Graphitic Carbon Nitride for Photocatalytic Hydrogen Evolution

Xinyu Zhang, Riping Liu, et al.

APRIL 22, 2020

ACS APPLIED NANO MATERIALS

READ 🗹

Get More Suggestions >